Multi-Megawatt Propulsion Based On A Compact Toroid Thruster

IEPC-2005-296

Presented at the 29th International Electric Propulsion Conference, Princeton University, October 31 – November 4, 2005

John Slough*
University of Washington, Seattle, WA, 98195, USA

Abstract: A research program in high power electric propulsion has been initiated with the primary goal being the experimental verification of the magnetic wave acceleration of a compact toroid plasmoid usually referred to as a Field Reversed Configuration. Based on previous laboratory results, multi-Newton thrust at high Isp (10 – 30,000 sec) can be produced by the rapid acceleration of a compact plasmoid driven by an externally applied propagating magnetic field accelerator. This paper includes a description of the concept, and the basic theory of operation including 2 D numerical calculations. A description of the experimental apparatus that has been constructed with results from initial operation of the magnets will also be presented.

Nomenclature

B	=	Magnetic field
B_{vac}	=	Vacuum magnetic field magnitude
B_{ext}	=	Magnetic field radially external to the FRC
E_x	=	Total energy in system "x"
φ_i	=	FRC internal closed (poloidal) flux
Φ_M	=	Magnetic potential of a dipole in a uniform field
F_z	=	Thrust in axial (z) direction
Isp	=	specific impulse (seconds)
J	=	current density
KE	=	Kinetic energy of moving object
L_x	=	Length of object "x"
m_d	=	Dipole moment of induced FRC diamagnetic current
m_i	=	Mass of plasma ion
M	=	Mass of FRC
μ_0	=	Magnetic permeability
N	=	Particle inventory of FRC
P	=	Plasma radial pressure
r_x	=	Radius of object "x"
T	=	FRC plasma total temperature ($T_e + T_i$)
T_{MPD}	=	Thrust of MPD thruster from Lorentz force
v_z	=	FRC axial velocity

All quantities are in SI units

*

I. Introduction

The rapid movement of large payloads, either for orbit maneuvering or interplanetary travel, imposes a demanding requirement for megawatt level propulsive power at significantly higher Isp than can be provided with chemical propellants. The high-power electric propulsion system to be described here can effectively meet the challenges of human and robotic space exploration with affordability, reliability and safety and enable missions not possible with other propulsion systems. The naturally high Isp of the magnetically accelerated plasmoid would operate with extremely low propellant consumption, considerably reducing the initial launch mass, vehicle scale and cost.

There has been a large variety of thruster concepts that have been developed for efficient operation at the kilowatt level. However, for the large thrust and relatively high specific impulse (Isp) needed for the missions considered here, the electromagnetic devices offer inherently high power densities needed. Electromagnetic plasma acceleration has in the past been a very attractive concept for a variety of high power space missions ranging from rapid orbital maneuvering to interplanetary travel. The power handling capability of the electromagnetic thruster arises from the Lorentz force thrust mechanism, i.e. the electromagnetic body force on plasma currents (**F** = **J** x **B)** to accelerate a propellant plasma.

At lower powers the plasma currents mainly heat the plasma through ohmic dissipation as in the electrothermal arcjet thruster. The electrothermal thrusters simply use a plasma discharge to add thermal energy to the propellant. By contrast, electromagnetic thrusters depend on electromagnetic forces generated in a very high-current plasma discharge (typically thousands of amperes) to accelerate the plasma propellant. The current density, J, produced in the plasma discharge has two effects. First, it ionizes the propellant, but more importantly, the high current produces a significant self magnetic field. It is the subsequent interaction of this magnetic field with the plasma currents that propels the plasma out of the thruster at high velocity (Isp). This dependence results in a thrust proportional to the square of the current, (J^2), and the thrust (and thruster efficiency) rises rapidly with current. Because the plasmas used are quasi-neutral, space charge limits do not apply. An externally applied field can also be added to increase the force.

Thrusters that employ electromagnetic acceleration, i.e. a large plasma current, whether it be with or without externally applied magnetic fields, can be operated as a sustained or pulsed discharge. Sustainment typically implies electrodes as this is the only way to maintain the large currents required. Up to now, there have been two electromagnetic thrusters that have received significant development as MW class thrusters - the Magneto-Plasma Dynamic (MPD) thruster[1], and the Pulsed Inductive Thruster (PIT)[2]. The Magnetically Accelerated Plasmoid (MAP) thruster that is the subject of this paper represents a new thruster that compares very favorably with these two, and holds the promise for a system that can significantly improve performance at the multi-MW level.

The most developed thruster in this class is the Magneto-Plasma Dynamic (MPD) thruster. This thruster type can be operated in either steady-state or pulsed mode. It has an axisymmetric geometry (annular anode surrounding a central cathode). The current generated by the applied voltage differential between the electrodes induces an azimuthal magnetic field, which in turn interacts with the current to produce an axially directed electromagnetic force. This electromagnetic component has traditionally been approximated by the Maecker formula[3]:

$$T_{MPD} = \left(\frac{\mu_0 J^2}{4\pi}\right)\left[\ln\left(\frac{R_A}{R_C}\right) + \delta\right] \qquad \frac{1}{2} \le \delta \le \frac{3}{4} \tag{1}$$

where the parameter δ is chosen based on the current distribution over the cathode surface. In steady-state operation the high current (kiloamps), low-voltage (100–200 V) arc discharge attaches diffusely to both electrodes. The majority of the plasma current is provided by thermionic emission from the hot cathode (> 2500 °K). The MPD thruster is capable of providing specific impulse Isp of 1000 – 12,000 s (10–120 km/s) with a peak efficiency of ~ 50% (depending on the propellant and power level). Both Isp and efficiency increase as power level increases. Lithium propellant has the best reported performance below 10 MW, and hydrogen produces the best performance above 10 MW.

The main challenges for the MPD thruster is its overall efficiency and electrode erosion. The electrode erosion is a problem for virtually all steady thrusters, but it is particularly an issue at high currents. With regard to efficiency, it is useful to examine the various loss channels for the MPD thruster as determined from a detailed characterization provided by the analysis of the two-dimensional flow-field computed by a resistive 2D MHD code (MACH2)[4]. A very similar code has been used to characterize the behavior of the MAP thruster, and the successful benchmarking

of the code with a well characterized thruster such as the MPD gives confidence that the code results will reflect the behavior of the actual MAP device as well.

Unlike the MAP thruster, the MPD produces a turbulent, low temperature plasma, and can be characterized by a low magnetic Reynolds number. In fact, it is key to its operation with or without an applied field. If the plasma were well magnetized, it would be difficult to liberate the plasma from the thruster fields. What is observed in the code is a much higher resistivity that provides for the plasma to flow rapidly across the magnetic fields. Two-dimensional current distribution comparisons determined that modeling with Spitzer transport is inadequate. In the MPD plasmas atom–electron collisions dominate causing a substantial increase in the plasma resistivity. The modeling results thus indicate incomplete hydrogen-propellant ionization, which increases the plasma voltage, but does not increase thrust. The dominant energy loss was calculated to be frozen-flow even though it decreased with increasing discharge current. Almost half the available power is not deposited into the plasma, and thus has no opportunity to be converted to useful thrust power. As power is increased, the increase in discharge voltage observed over the calculated plasma voltage from MACH2 implies that there is an increasing power deposition to the electrodes. Part of the difficulty lies in the fact that for the MPD thruster, the nozzle (anode) plays an integral part of the discharge process. The frozen flow losses can not be easily addressed by a change in the nozzle shape and dimensions without changing the discharge characteristics. MAP is an electrodeless thruster where there is sufficient time for full preionization. In the MAP thruster such issues will not arise as the frozen flow losses can be addressed by an appropriate magnetic nozzle that is separate from the plasma formation and acceleration.

The other type of electromagnetic propulsion devices can be described collectively as pulsed inductive accelerators. Inductive plasma accelerators are attractive as propulsive devices for several reasons. The lifetime and contamination issues associated with electrode erosion in conventional plasma thrusters (Ion, Hall, and MPD) do not exist in devices where the discharge is inductively driven. In addition, a wider variety of propellants (e.g. ammonia CO_2, H_2O) can be used as compatibility with metallic electrodes is no longer an issue. Moreover, pulsed inductive accelerators (indeed, pulsed thrusters in general) can maintain the same performance over a wide range of input power levels by simply adjusting the pulse rate. With pulsed inductive plasma accelerators, energy is stored in a capacitor and then discharged through an inductive coil (or a series of coupled coils as in MAP). These axisymmetric devices are electrodeless, where the large currents are induced in a plasma located some distance away from the induction coil. The plasma is accelerated axially and expelled at a high exhaust velocity through the interaction of the induced azimuthal plasma currents and the radial component of the coil magnetic field.

There are two concepts which operate on this principle and have demonstrated experimentally the capability of operating at multi-megawatt power levels. One is the MAP thruster based on the Field Reversed Configuration (FRC), and the other is the Pulsed Inductive Thruster (PIT). Both the FRC and PIT thruster have been operated at MW power levels for single pulses. In previous experiments, the acceleration of the FRC plasmoid was primarily for fusion studies[5], which have produced thrust powers many times that of the PIT device, and at velocities greater than 300 km/sec (I_{sp} = 30,000 sec). The primary purpose of the MAP experiments is the optimization of the FRC for propulsion which will be described in greater detail in the next section. However, it is worth reviewing the PIT device, as with the MPD, to understand more clearly the unique advantages of MAP.

The PIT employs a large, flat, spiral wound induction coil that is on the order of a meter in diameter. Given the inherently small region of strong interaction with the induction coil, the coil current pulse lengths are typically on the order of microseconds. The PIT operates by first flowing gas onto the coil surface from a central mass injection pylon. Once the gas has been injected, a bank of high-voltage (~10 kV), high-energy storage (~ 10 kJ) capacitors is discharged providing a large azimuthal current pulse to the coil. This rapid change in magnetic flux produces an azimuthal inductive electromotive force at the coil's surface. The induced electric field ionizes the gas, resulting in an azimuthal current flow in the plasma. The interaction of this current with the coil field accelerates the plasma away axially. Several experimental studies, as well as theoretical analysis using the MACH2 code, have determined an optimum PIT thruster performance. Specific impulses up to 8000 s and efficiencies on the order of 50% have been measured in the single pulse mode. There is only a limited range of improvement however, with performance most likely decreasing at increased power (or equivalently for a pulsed thruster, increased discharge energy). A measure of performance for a pulsed thruster is the impulse bit. For the PIT:

$$\int F_z dt \sim \int_{pulse} \int I_{coil}^2 e^{-z(t)} dt \qquad (2)$$

As indicated earlier, for any improvement in impulse bit and thrust efficiency, the current must peak while the plasma current sheet is still close to the accelerator coil (i.e. near z = 0). The force accelerating the sheet drops exponentially as the sheet moves away, even if the peak current is maintained. Therefore, to achieve efficient pulsed

inductive acceleration, the highest possible peak current must be reached before the sheet moves far from z = 0. This implies that any attempts to lower the peak current and extend the current pulse length will result in a less efficient acceleration process with a higher fraction of the total energy lost in the circuit through resistive dissipation. These limitations do not apply to the MAP thruster as the current pulse travels with the plasmoid in the accelerator, always maintaining close proximity to the plasmoid. A description of how this process is realized experimentally will now be given.

II. The Magnetically Accelerated Plasmoid (MAP) Thruster

A. Physics of the FRC plasmoid propellant

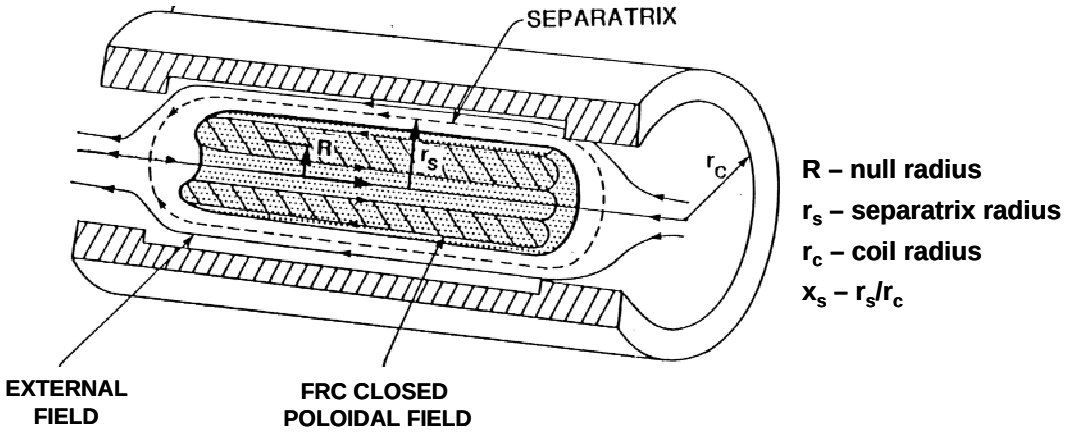

Figure 1. The Field Reversed Configuration (FRC)

The MAP thruster, when completed and operated as planned could potentially represent the highest power electric propulsion device yet devised. This is made possible by the unique attributes of the plasma propellant that is at the heart of the thruster, the Field Reversed Configuration (FRC). The FRC is a compact toroidal plasma (plasmoid) that is magnetically self confined by a poloidal magnetic field generated by toroidal plasma currents alone (see Fig. 1). It has topologically the simplest closed field line structure and the highest equilibrium β (the ratio of plasma to magnetic energy density) of any magnetically confined plasma. The FRC equilibrium is characterized by the following relations[6]:

$$\text{Radial Pressure Balance}: \quad P_0 = n_0 kT = \frac{B_{ext}^2}{2\mu_0} \tag{3}$$

$$\text{Axial Pressure Balance}: \quad \langle\beta\rangle = \int_0^{r_s} \frac{2\mu_0 P(r)}{B(r)^2} dr = 1 - \tfrac{1}{2} x_s^2 \tag{4}$$

$$\text{Flux Conservation}: \quad B_{ext} = \frac{B_{vac}}{(1 - x_s^2)} \tag{5}$$

The FRC is typically formed in a simple cylindrical coil slotted axially to allow for the introduction of azimuthal (θ) currents. The initial axial magnetic field is populated with a weakly ionized plasma which is then rapidly reversed. The rapid reversal induces large θ currents that fully ionize the gas and encapsulate the plasma in a closed field region. The continued increase of the external axial magnetic field isolates the newly formed FRC from chamber (thruster) walls (see Figure 1). The magnetic separation of the thruster from the plasma essentially eliminates thermal losses from the plasma to the rocket. The high energy density and magnetic isolation make the FRC plasmoid ideal for propulsion, but it also makes it a very good candidate for magnetic fusion energy. In fact it is in this context that much of the research on FRCs has been conducted. Its use for propulsion may be new, but there is a large body of research on the FRC that can be tapped for the advancement of the concept as a thruster.

To understand the MAP concept better, it is useful to review the manner that the FRC has been generated in past experiments. There are several methods that have been devised to form the high β FRC plasma. These include field reversal with beam currents, merging of spheromaks, and reversal by currents driven by a rotating magnetic field. There is however only one technique that has proven capable of producing a high energy plasma in a high magnetic field, and one that is particularly well suited for the purpose of propulsion. This technique is commonly referred to as reversed field theta pinch formation. It was the first technique to produce keV plasmas with energy confinement times many times the Alfven time. A brief discussion of the method will now be given, as a variant of it is employed on the MAP thruster.

The plasma is generated by a sequence of events as indicated graphically in Fig. 2. The following steps in formation are:

1) A weakly ionized gas is produced in an axial magnetic field. This field is usually referred to as the reverse bias field.

2) Voltage is applied to the coil reversing the direction of B. The induced E_θ generates a strong ionizing current that prohibits the loss of the initial axial field now referred to as the trapped reversed field.

3) Increasing (forward) axial field now provides for the formation of the FRC plasma. Forward flux equal to the trapped reversed flux forms closed flux surfaces inside the vacuum chamber. Plasma can now flow on these field lines from the inner (reversed) field to the outer field and relax into a 2D radial equilibrium distribution.

4) Further field (flux) increase radially compresses and heats the FRC. This additional field is now external to the FRC plasmoid. The closed field line FRC contracts axially into a high β equilibrium to counter the compressional effect of the external axial field.

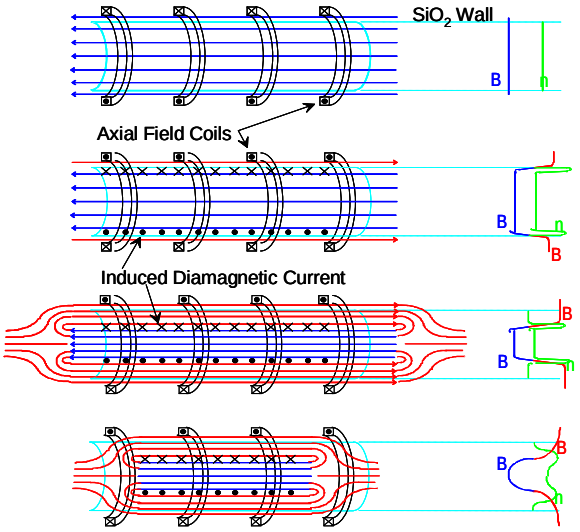

Figure 2. FRC Formation Sequence: *See text for description of each step.*

With the sequence illustrated in Fig. 2 a magnetically isolated plasmoid is formed that is neutrally stable to axial translation if the external guide field is uniform. By producing a magnetic field gradient axially across the FRC plasmoid, the directed velocity of the FRC can be increased. In previous experiments FRCs of near milligram mass were accelerated to velocities of 2×10^5 m/s in a single pulse. The ejection of the plasmoid by an external axial field also avoids the serious problem of detachment which could occur in thrusters that employ a magnetic mirror or magnetic nozzle. The ejection of hot, highly conductive plasma on thruster magnetic fields would result in larger frozen flow losses as field lines would need to tear and reconnect outside the thruster carrying away magnetic energy with no thrust.

The simplest manifestation of an FRC based thruster is that obtained by employing a conically shaped flux coil for the formation, acceleration and ejection of the FRC. The development of a novel inductive magnetized plasma source called IMPAC (Inductive Magnetized Plasma Accelerator) was undertaken to investigate the possibility of producing and accelerating FRCs at a very high pulse repetition rate by using solid-state switches, lower voltage capacitors, and a simple formation technique[7]. By forming the FRC in an axially tapered coil as was done with IMPAC, an FRC is simultaneously formed and accelerated. The final velocity is determined by several experimental control "knobs". In addition to a variable fuel mass, the repetition rate at which new FRCs are formed and ejected determine the thrust. There is thus a very wide range in both thrust and Isp achievable with minor changes in formation fields, timing, and fuel. There is continuing work on this type of plasmoid thruster at NASA Marshall on the PTX device[8]. The discussion of the IMPAC results is made more to illustrate that the repetitive operation of a high energy FRC thruster can be accomplished with current technology. What is needed is the demonstration and measurement of thrust and Isp in a configuration that can take full advantage of the FRC plasmoid propellant as in the MAP thruster.

B. Physics of the MAP accelerator

As has been stated, the acceleration of the FRC is obtained by creating an axial magnetic field gradient across the FRC. Sustaining that axial gradient via a traveling magnetic wave allows for the FRC to be accelerated to an arbitrarily high velocity and thrust. A disadvantage of the PIT, and for that matter IMPAC, is that the duration of the magnetic push is determined by the coil geometry to be transient and short range. There is no method to continue the acceleration process once the plasma current ring is any distance away from the driver coil. In MAP the process of continued acceleration is made possible by a propagating magnetic wave.

It should be mentioned that there is a significant additional source of directed energy represented by the large internal energy of the FRC that does not exist for the other thruster concepts. For the FRC, after the acceleration in the propagating wave field, the final ejection and expansion of the FRC at the end of the accelerator provides for a mechanism to convert the internal energy of the FRC, both thermal and magnetic, into directed thrust. This must be accomplished by an appropriately designed magnetic nozzle. There is advantage here as well for the MAP FRC as the expansion is not involved in the ionization and current formation processes. The resistive losses and frozen flow losses are thus minimized. It is useful in analyzing the various physical processes to separate these two different sources of thrust power, and treat each one separately. The MAP experiment was designed to study the two different mechanisms separately as well. In this way a better understanding of the physics of each process can be obtained, and the optimization can be addressed without the complication presented with overlap. This is not possible in the case of the conical FRC thruster, but it will be seen that general remarks about the expansion and conversion process will apply equally to this simple thruster as well. The basic formation and translation of the FRC out of a solenoidal coil will be considered first as it is the easiest to analyze. It has also been well diagnosed and documented in previous FRC experiments[9].

To begin, consider the system illustrated in Fig. 3 in which an ellipsoidal, perfectly conducting body of minor radius r_s is expelled by a magnetic field of a hollow conducting shell of radius r_c. Assume that initially the conducting body has a negligibly small drift that eventually causes the body to reach and experience the field gradient at the end of the solenoid. If resistive losses are neglected, the total energy of the system before and after the body is expelled from the solenoid does not change. If the object is incompressible, one has:

$$\frac{B_{ext}^2}{2\mu_0}\pi\left(r_c^2-\langle r_s^2\rangle\right)L_s-\frac{B_{vac}^2}{2\mu_0}\pi\langle r_s^2\rangle L_s=\frac{1}{2}M v_z^2 \qquad (6)$$

where $\langle r_s^2\rangle$ is the average surface radius along the projectile length L_s. M is the mass of the body, and v_z is the axial velocity acquired in ejection. From Eqs. (5) and (6), the kinetic energy imparted to the projectile is:

$$KE = \frac{B_{vac}^2}{2\mu_0}\left(1-\langle x_s^2\rangle\right)\pi r_c^2 L_s = E_{BV}\left(1-\langle x_s^2\rangle\right) \qquad (7)$$

where the E_{BV} is the vacuum magnetic energy inside the coil after ejection. Maximum energy transfer to the projectile is obtained for the largest vacuum field, and for the smallest (highest density) projectile. The purpose of this exercise is to point out that the shape of the field region, or detailed knowledge of the induced skin currents in the conductor are not needed to understand or calculate the conversion of stored magnetic energy into translational motion. The projectile final motional energy is completely determined by the initial conditions. The question now becomes, how does this picture change by having the projectile be a compressible object with significant internal energy? The expansion and ejection of such an FRC-like object is also indicated in Fig. 3.

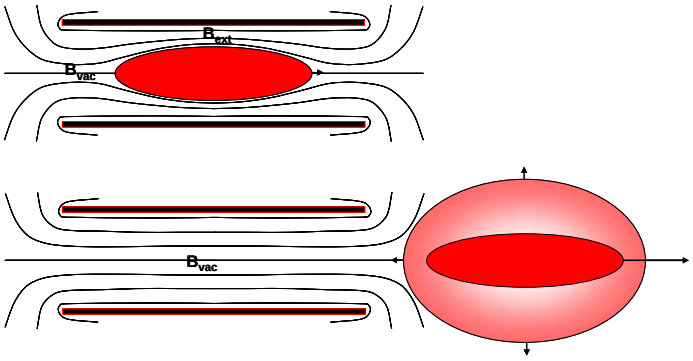

Figure 3. Ejection of a conducting body from a flux conserving coil. *Initial state represents equilibrium with a small drift to the left.*

The total energy inside the flux

conserving boundary includes the magnetic field energy as before, but there is now an additional term that represents the FRC internal energy. From radial pressure balance (see Eq. (3)) the product $n_i kT$ must balance the external magnetic pressure in equilibrium. Using this relation for B_{ext} in Eq. (5), combined with the average β relation (Eq. (4)), one can write for the total energy at any time within the flux conserver as:

$$E_{Tot} = \tfrac{5}{2} NkT + E_{BV} + \tfrac{1}{2} Nm_i v_z^2 \qquad (8)$$

where T is the total plasma temperature N represents the ion inventory inside the FRC separatrix ($N = n_i \cdot vol$), and m_i is the ion mass so that $Nm_i \cong M$. From this equation it is apparent that the internal energy is composed of two terms; one reflecting the thermal energy of the FRC plasma ~ 3/2NkT, and the other reflecting the internal magnetic energy ~ NkT. If the no external magnetic field change is affected during the translation and ejection of the FRC (no change in the system total energy), $\theta \equiv 5kT + m_i v_z^2$ is a constant. If the expansion of the plasma as it exits is adiabatic, then the axial kinetic energy gained by the FRC will come at the expense of expansion cooling. From the conservation of energy (θ = a constant) then the following relation may be obtained:

$$KE = \tfrac{1}{2} Mv_z^2 = \tfrac{5}{2} N k \Delta T \qquad (9)$$

where $\Delta T = T_0 - T_{ej}$ is the change in plasma temperature from its equilibrium value, T_0, inside the coil to that after ejection and expansion, T_{ej}. This equation is significantly different than the relation for a solid projectile. Here the propulsive energy is only a function of the enthalpy of the FRC plasma generated during formation. The conversion of this internal energy is dependent on how the FRC is ejected. The expansion needs to be adiabatic in order to minimize frozen flow losses i.e. $T_{ej} << T_0$. Therefore, a suitable magnetic nozzle must be designed to yield the maximum transfer of FRC internal energy into thrust energy. Eq. (9) will still be valid for the conical θ pinch thruster since it is essentially nothing more than an overlap of the FRC formation, heating, and expansion that is represented by Eq. (9). A discussion of the dependence of the internal FRC energy on various experimental parameters related to FRC formation could be carried out, but this is not warranted at this point as the main method for adding translational energy to the FRC in MAP will be in the form of acceleration by a traveling magnetic field configuration.

Considerably higher directed energies can be attained if the FRC is resonantly pushed by a traveling magnetic wave. This situation is depicted in Fig.4 with the field pattern following the FRC with the same steadily increasing velocity. If one assumes that a quasi-steady picture develops similar to that in Fig. 4 during the acceleration, the FRC can be treated as a stationary object much like the projectile in the first example. Determining the force on the FRC is thus reduced to determining the force from the external magnetic field on a magnetic dipole that represents the current that is induced in the FRC in response to the application of the inhomogeneous magnetic field.

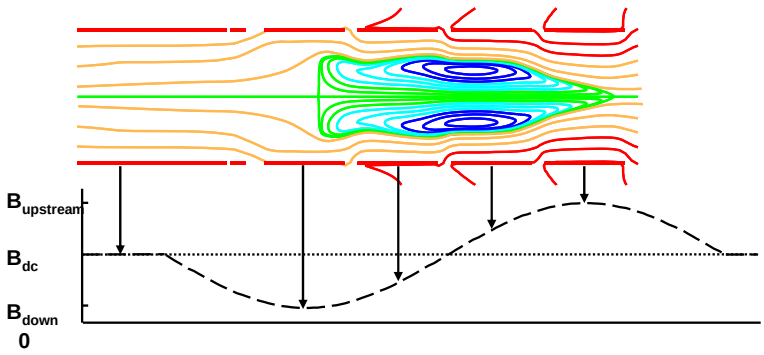

Figure 4. FRC acceleration process with sequenced coils. *Upper plot of flux contours taken from numerical calculations for discharge 1647 during the acceleration of an FRC at UW. Bottom plot illustrates phasing of the accelerator coils. Each coil in turn is switched on for one complete cycle. The phase of each coil at time of calculation is indicated by arrow.*

This simplification is supported by the 2D MHD calculations of the magnetic traveling wave acceleration. The diamagnetic plasma currents responsible for the FRC equilibrium are found to be small compared to the sheath currents that flow in response to the magnetic perturbation introduced by the propagating magnetic pulse. The force on this current loop by the external magnetic field is given by:

$$\mathbf{F} = M\frac{d\mathbf{v}}{dt} = \nabla(\mathbf{m}_d \cdot \mathbf{B}) \qquad (10)$$

where dipole moment, $\mathbf{m}_d$, is the magnetic dipole moment induced by the field in the diamagnetic FRC of mass M. Using the vector identity:

$$\nabla(\mathbf{m}_d \cdot \mathbf{B}) = \mathbf{m}_d \times (\nabla \times \mathbf{B}) + (\mathbf{m}_d \cdot \nabla)\mathbf{B} \qquad (11)$$

, and recognizing that in the vacuum surrounding the FRC that $\nabla \times \mathbf{B} = 0$, one has

$$\mathbf{F} = M\frac{d\mathbf{v}}{dt} = (\mathbf{m}_d \cdot \nabla)\mathbf{B} \qquad (12)$$

It is possible to get an approximate expression for the induced dipole moment by considering the much simpler case of a conductor in a homogeneous axial magnetic field as in Fig. 5. The magnetic scalar potential for a spherical conductor can be readily obtained from Laplace's equation. The solution for a perfectly conducting diamagnetic sphere (magnetic field separatrix coincident with sphere surface) in a homogeneous field, B_{vac} is:

$$\phi_M = \frac{B_{vac}}{\mu_0} z\left(1 + \frac{r_s^3}{2(r^2 + z^2)^{3/2}}\right) \qquad (13)$$

where r_s is the sphere radius. The first term corresponds to the potential of the homogeneous field. The second corresponds to that of a dipole parallel to the z axis with a moment:

$$\mathbf{m}_d = -\tfrac{1}{2} r_s^3 \frac{\mathbf{B}_{vac}}{\mu_0} \qquad (14)$$

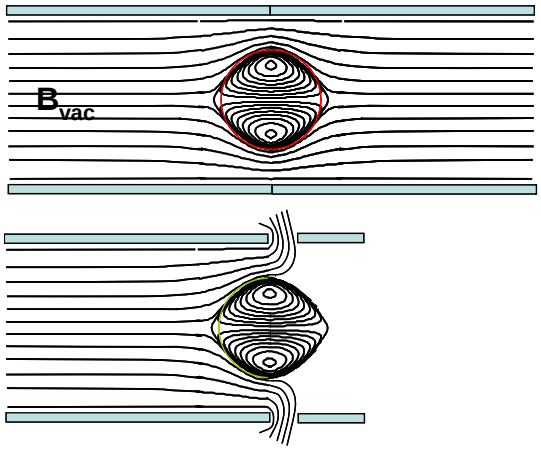

Figure 5. Force on a dipole conductor. *(top) Diamagnetic spherical FRC in uniform field. (bottom) same FRC but in inhomogeneous field*

With the purely axial nature of the magnetic moment, the axial component of the magnetic force stated in Eq. (12) can be reduced to:

$$F_z = m_d \cdot \nabla B_z = m_d \frac{\partial B_z}{\partial z} \qquad (15)$$

There is no net axial force on the FRC, regardless of shape, in a homogeneous field. The force from the +z side is countered by the force from the –z side. If one assumes the ideal driving magnetic waveform, also depicted in Fig. 5, the maximum force will derived. The approximation that the shape of the end of the FRC residing in the driving coil being hemi-spherical is a reasonable enough based on the numerical calculations. Changes in shape from other than hemi-spherical will change slightly the numerical coefficient for m_d given in Eq. (14), but the basic scaling will be the same. The approximation that the downstream field pressure negligible compared to the driving field should also be close to what can be achieved in the actual thruster. What is left is to determine the dependence of the FRC separatrix radius on the magnitude of the driving field. This depends somewhat on the internal magnetic profile. The profile that most closely fits the FRC equilibrium measurements is that generally referred to as the rigid rotor (RR) profile ($J_\theta(r) \propto n\omega r$). In this case, the closed poloidal flux, φ_i, is given by the following expression:

$$\varphi_i = \frac{\pi}{2\sqrt{2}} \frac{B_{ext}}{r_c} r_s^3 \qquad (16)$$

The magnitude of the dipole moment of the FRC can now be stated in terms of the trapped poloidal flux inside the FRC:

$$m_d = \frac{\sqrt{2}}{\pi} r_c \varphi_i (1 - x_s^2) \qquad (17)$$

where Eq. (5) was used to relate B_{ext} to B_{vac}. The constraints placed on the magnitude of the FRC magnetic moment, as well as the axial field gradient, relate to what has been achieved in previous FRC experiments. It is entirely possible that improvements in these parameters can be made, but a scaling relation based on previous results

provides for a more conservative assessment of the device. A comfortable maximum internal FRC flux for previous FRC experiments of various size is given by the normalized field:

$$\frac{\varphi_i}{\pi r_c^2} \cong 0.05 \text{ T}. \tag{18}$$

In addition, the axial gradient scale length has as a practical minimum, - that given by the length over which the external coils can generate a large ΔB change between them. Again, a practical minimum would be $\Delta z \sim 2r_c$. Assuming this, one has:

$$F_z \sim m_d \frac{\Delta B_z}{\mu_0 \Delta z} = 5.6\text{x}10^4\, r_c^3 (1 - x_s^2) \frac{B_{ext}}{2r_c} = 2.8\text{x}10^4\, r_c^2 B_{vac} \tag{19}$$

The work done by the accelerator fields on the FRC in traveling a distance d along the accelerator is $F_z \cdot d$, and is equal to the kinetic energy acquired by the FRC. The total directed kinetic energy acquired from an accelerator of length L_a is then:

$$\tfrac{1}{2} M v_z^2 = 2.8\text{x}10^4 L_a r_c^2 B_{vac} \tag{20}$$

This result is within 10% of the values obtained with the more accurate 2D numerical results to be discussed in the next section. It would appear from this result that the directed energy scales with B not B^2 as one might expect. The B^2 dependence is actually there implicitly as the relative magnitude of the FRC flux was assumed in Eq. (18), and its field dependence suppressed. It can be seen that the directed energy scales linearly with the accelerator volume. The thrust power as well as thruster efficiency can be increased by extending the accelerator length. This is because the magnetic energy required does not need to be present simultaneously throughout the accelerator. The accelerating field that appears in Eq. 20 can be only at the upstream end of the FRC as it is in a traveling wave. The accelerator is thus more like a lossy transmission line that pushes the FRC along within it. The decay of the pulse and the extraction of energy from the field occur primarily at the end of the accelerator as it is proportional to the FRC velocity.

C. 2D MHD Calculations of MAP

A series of calculations were undertaken with the resistive 2D MHD code Moqui[10]. This is a code that shares a similar heritage with the MACH2 code, but has been customized particularly for FRC physics and geometry. This code has been used extensively to study the formation and translation of FRCs. The Moqui code has proven itself as an invaluable tool during the design phase of FRC experiments. Moqui employs an Arbitrary Lagrangian/Eulerian (ALE) algorithm, whereby the grid can be stationary in the laboratory frame (Eulerian), move with the fluid (Lagrangian), or move in some other arbitrary manner. In Moqui, an adaptive algorithm is tuned so that the grid is heavily concentrated in the regions both of steep gradient and in the vicinity of the FRC. This feature greatly enhances the accuracy of the calculations by making the cell size smallest where it is most needed. Even more important in the case of translated FRCs, the grid tends to translate with the FRC minimizing the contribution from the convective derivative, which tends to be very diffusive. To accomplish this, Moqui has an

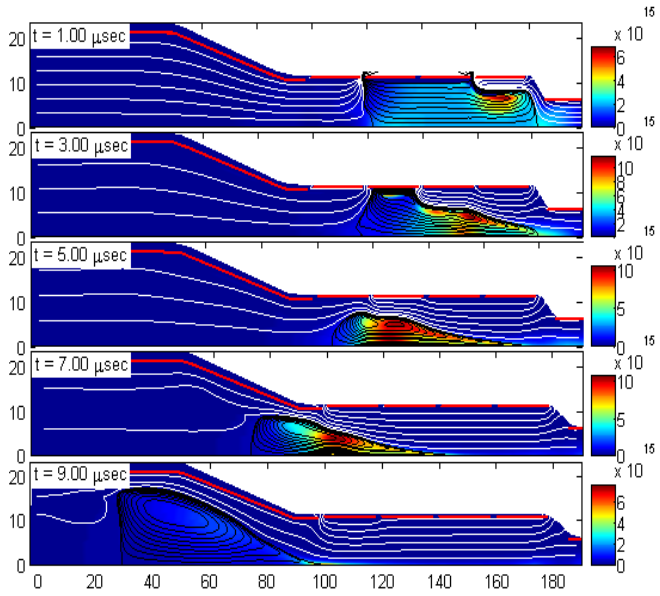

Figure 6. Flux and density contours for a numerical calculation of the MAP thruster with magnetic nozzle. *Black lines are flux contours in the FRC. Axis and density bars are in units of* cm^3**.**

algorithm that locates the FRC and concentrates the grid in that region.

From Eqs. (9) and (20) it would appear that the directed energy increases with thruster size. Previous experimental work defined to some degree the boundaries for MAP. For several practical reasons it was decided that the maximum coil voltage would be ~ 10 kV, and the maximum operating gas fill would be 4 Pa (30 mTorr) typical of previous FRC experiments where long lived FRC have been routinely formed. ($\tau_N >> \tau_A$). The voltage is also within range of series operated solid state switches for future rep rated operation. The coil radius of ~ 0.1 m was chosen again based on the wealth of experimental data that exists for this size, as well as the fact that it is large enough to achieve multi megawatt thrust power with a rep rate of less than 1 kHz. The accelerator length was variable, with increasing length reflecting a nearly linear increase in FRC exit velocity. The accelerator length was based on a length that was sufficiently long to provide a solid test of the theory, yet kept the final FRC kinetic energy below 5 kJ to minimize possible damage to internal diagnostics and vacuum boundaries. The MAP thruster numerical calculations were conducted using these constraints. The results shown in Fig. 6 show the formation, acceleration, and expansion/ejection of the FRC. Key parameters are plotted in Fig. 7. It is noteworthy to observe that the heating of the FRC while it is in the accelerator section of the thruster (~ up to 7 μsec) is converted to directional energy by the magnetic nozzle during expansion. There is only ~ 150 J of thermal energy remaining in the FRC at the end. This is compared to the directed energy KE ~ 3.3 kJ. The frozen flow loss is thus quite negligible.

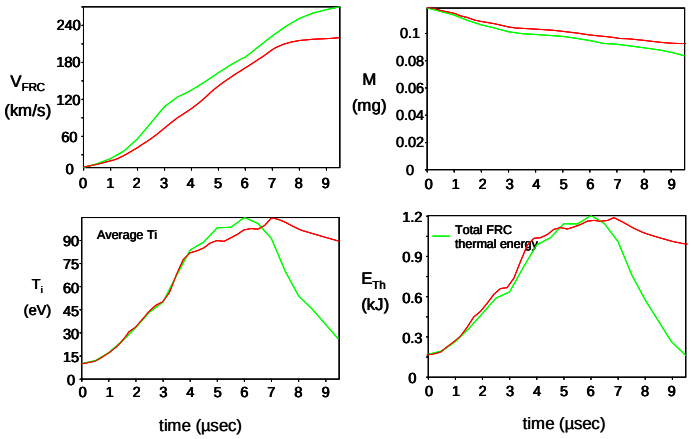

Figure 7. Comparison of various global parameters for the MAP thruster with and without magnetic nozzle. *Time period covers the FRC formation acceleration. and ejection for the calculations shown in Figs. 6 and 8. Red line indicates calculation without a magnetic nozzle. This case (Fig. 8) has a passive coil at the exit of the thruster, and is similar to the initial experimental design.*

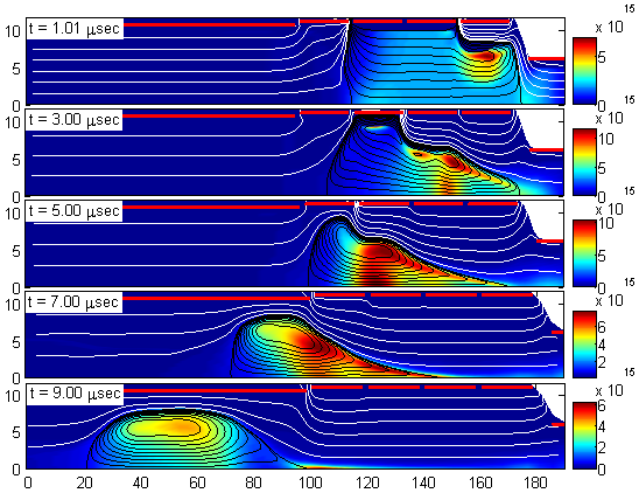

Figure 8. Flux and density contours for a numerical calculation of the MAP thruster as constructed for initial acceleration experiments. *Black lines are flux contours in the FRC. Axis and density bars are in units of cm.*

The formation and accelerator coils overlap to some degree, as this leads to the minimum formation time which minimizes the FRC losses. It also acts as a better representation and match of the coil rise time to that of a propagating wave transmission line. This manner of generating the driving magnetic field waveform is ultimately the goal for the thruster. For the initial experiments, the field is propagated by a sequential discharging of the magnets. This is also how the code was operated as well. A future upgrade to both code and experiment will be the formation of a discrete traveling wave as was done in the Propagating Magnetic Wave Accelerator (PMWAC) demonstration experiments[11]. The initial experiments will not have a magnetic nozzle section. This simplifies the implementation of the accelerator as a large dielectric chamber is not required to house the larger nozzle structure. It also allows for the evaluation of the accelerator efficiency independent of the nozzle physics. A numerical calculation based on the actual experimental design is shown in Fig. 8. A

comparison of the various plasma parameters is also shown in Fig. 7. It is clear from the difference in final FRC velocity achieved that the conversion of FRC internal energy results in additional directed energy, but that most of the energy is acquired from the direct acceleration of the FRC, even with the relatively short accelerator to be employed here.

A significant advantage in having a drift chamber rather than the nozzle expansion initially is that a much better measure of the FRC propellant thrust and Isp can be made on a plasma that is in a relative equilibrium state. Both internal and external magnetic probes as well as side-on interferometry and emission measurements, together with the code results should provide for a very accurate determination of the thrust power. This is important in that a conventional thrust stand measurement would be difficult to make with this thruster.

III. The MAP Experiment

This section provides a description of the experiment that has been constructed to explore the MAP concept. The experiment has just begun to collect data, mostly calibration and shakedown of the high voltage magnetics. The experiment can be broken down into several subsystems. Each of these will be briefly described, and where appropriate, the most recent data will be presented.

A. High Voltage Power Supply and Magnetics:

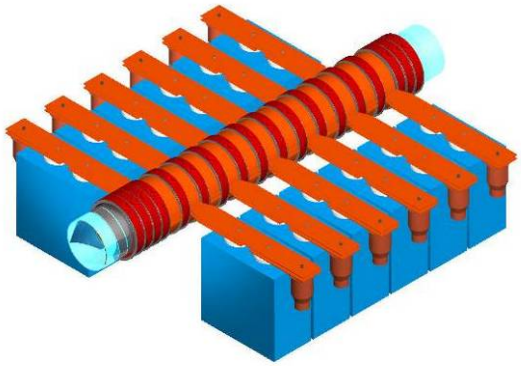

Figure 9. Schematic of the MAP discharge tube with fast magnet modules.

A propagating magnetic wave accelerator will be the simplest and most efficient method to accelerate FRC plasmoids. The first priority however was the formation of the optimum plasmoid in terms of mass and energy. The technology should not take priority over the physics at this point of development. The maximum flexibility and the broadest range of parameter space that can be accessed must remain the highest priority. For these reasons the prototype accelerator was designed with the utmost flexibility in design and operation. By having individual control in coil timing and waveform, the full capabilities of the MAP can be explored. A 3D schematic of the coil system is shown in Fig. 9. The code work was based on only four accelerator coils to minimize the numerical dissipation from grid rezoning across coil boundaries. There was no reason to limit the number in the experiment to less than could be conveniently connected to the vacuum tube. The coil width used in the experiment is roughly half of that used in the calculations (1 coil every 10 cm. for the experiment). Allowance was made for up to 12 individually supplied coils as in Fig. 9. The first implementation uses eight coils with the equivalent total length the same as in the calculations. Sequencing the start axially in pairs would give the same spatial and temporal waveforms as the calculations for comparison purposes. A finer control on the waveform can be obtained in the experiment however. A schematic of each coil module is shown in Fig. 10.

The MAP thruster employs ignitron ignitors and associated circuitry for the precise (~ 20 nsec) timing of the individual coil modules. The single turn magnet coils were fabricated from braided wire. This allowed for their easy placement and minimum gap between the flux boundary and the plasma tube. Although the preionized plasma is near the wall for a fraction of a μsec, the close

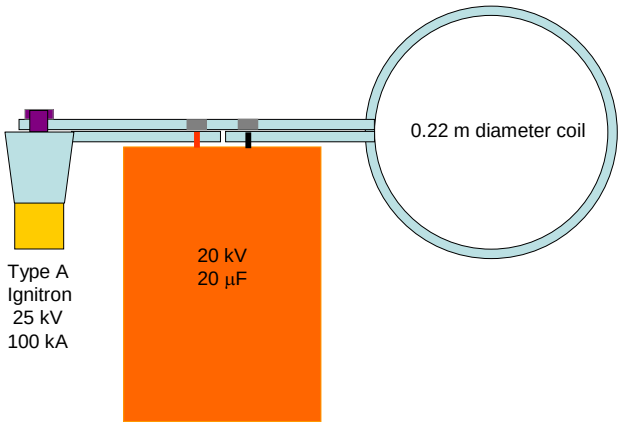

Figure 10. Coil module schematic for fast coils on MAP. (one of eight)

coupling significantly reduces flux loss through the plasma sheath as well as well as thermal transfer to the wall. The use of braided wire for the magnet coil also makes it easy to assemble and route the magnets to the feed plates. Conventional "shrink" tubing provides adequate high voltage protection.

An inductively isolated bias capacitor was employed as in previous FRC devices. A schematic of the circuit for a coil module with bias is shown in Fig. 11. The values for the various circuit elements have been obtained from testing of the actual coil modules. The bias module provides for the ability to have a reverse field for an extended period for preionization. A much more efficient preionization can come from the use of the fast module bank itself operated in what is referred to as second half cycle (SHC) operation. Here the bias field is introduced in the same direction as the eventual accelerating (forward) field (see Fig. 12). The fast module is then discharged so as to reverse this field producing the reversed field on the first half cycle. The bank continues to ring up producing a forward field that forms the FRC and drives the FRC axially down the accelerator as in the calculations. With each axial field zero-crossing from the fast module a large azimuthal current is induced that rapidly ionizes the background gas.

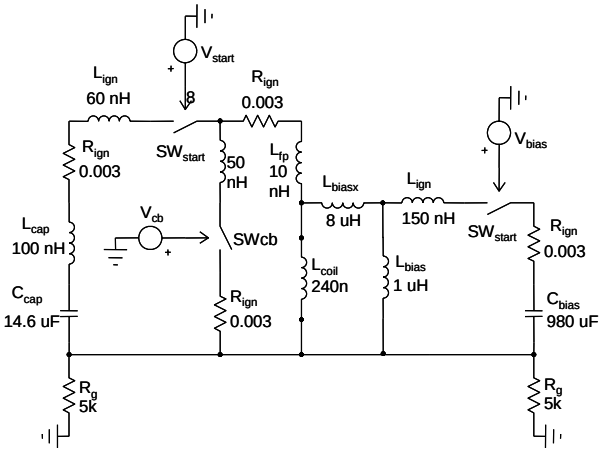

Figure 11. Circuit schematic for a single coil module with bias on MAP. *Circuit paramaetric values were experimentally determined.*

The double zero-crossing that occurs with SHC operation makes it an efficient preionizer and traps the maximum field possible for obtaining the largest FRC flux and heating. Even though a fast module SHC would have a somewhat smaller peak magnetic field amplitude compared to the FHC, having a forward rather than reversed bias more than makes up for the difference as can be readily observed in Fig. 12. For the conversion of current into field magnitude (Tesla) one divides the current by roughly 100. The waveforms shown in Fig 5-6 are that for a 20 kV capacitor charge so that the peak driving field can be greater than 1 T. For the MHD calculations the assumed field swing was 0.8 T.

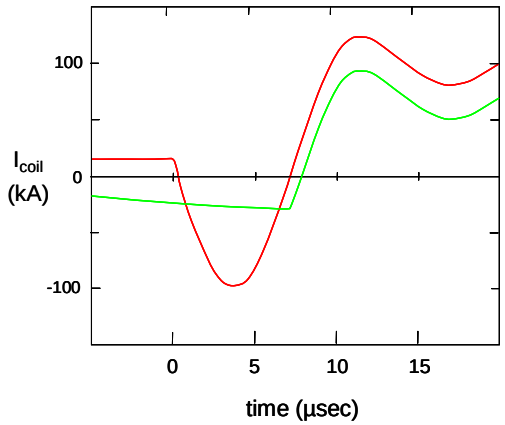

Figure 12. Current waveforms for first and second half cycle (SHC) operation of a single coil module on MAP. *The SHC red trace is the mode that being used incurrent experiments on MAP.*

The FRC plasma shape and size will be obtained by an array of magnetic loops placed in the central gap in each of the fast modules (see Fig. 13). The magnetic coils come as a pair where one loop encircles the tube at the coil radius, and measures the total flux of each coil. The other loop is a hairpin loop that extends around the tube circumference before folding back on itself. The flux through this loop provides a measure of the local external axial field at the tube wall of each coil. For a vacuum discharge of the magnets the field at the edge is the same as that as the rest of the coil in the approximation that the coil is much longer than the radius. This is the usual assumption that is made for a field reversed θ-pinch coil. Using the measured value of the field at the edge and the flux measured by the flux loop, one can determine how much flux must have been excluded by the presence of the FRC to increase the external field given the measured flux. In this manner the excluded flux radius, $r_{\Delta\varphi}$ ($\cong$ separatrix radius, r_s) at each loop pair can be determined. For the case of a series of short coils as is found on MAP, a bit more work must be done.

In this case knowledge of how the flux changes in vacuum as the coils are sequenced can be used to help determine the separatrix shape with plasma present. The separatrix shape can be approximately known by a method where the excluded flux radius $r_{\Delta\varphi}$ at a given axial position is calculated from the local magnetic field B_z and flux φ measurements at the vacuum coil wall. That is,

$$r_{\Delta\varphi} = r_{loop}\sqrt{1-\frac{\varphi_p B_{zvac}}{\varphi_{vac} B_{zp}}} \tag{21}$$

where the subscripts vac and p correspond, respectively, to the vacuum and plasma shots, and r_{loop}, is the flux loop radius. The axial $r_{\Delta\varphi}$ profile of the FRC is formed using an axial array of magnetic probes and flux loops along the vacuum vessel using this formula. However, it is known that the profile does not show a true separatrix shape at the ends since uniformity of the magnetic field is still assumed in Eq. 21. For the drift chamber section of the MAP experiment this will be quite accurate, as the entire length of this section is surrounded by a split copper flux shaper (see Fig. 13). In order to determine separatrix shape more precisely during acceleration, a deconvolution method will be employed in which the measured magnetic fields are compared with those generated by fixed currents assumed to be flowing in the FRC. In addition, an iterative method has been determined for calculating the separatrix shape with high accuracy[12]. Using this iterative method it also becomes possible to solve the Grad–Shafranov equation from the separatrix shape and the edge parameters and thereby infer the magnetic structures inside the separatrix as well.

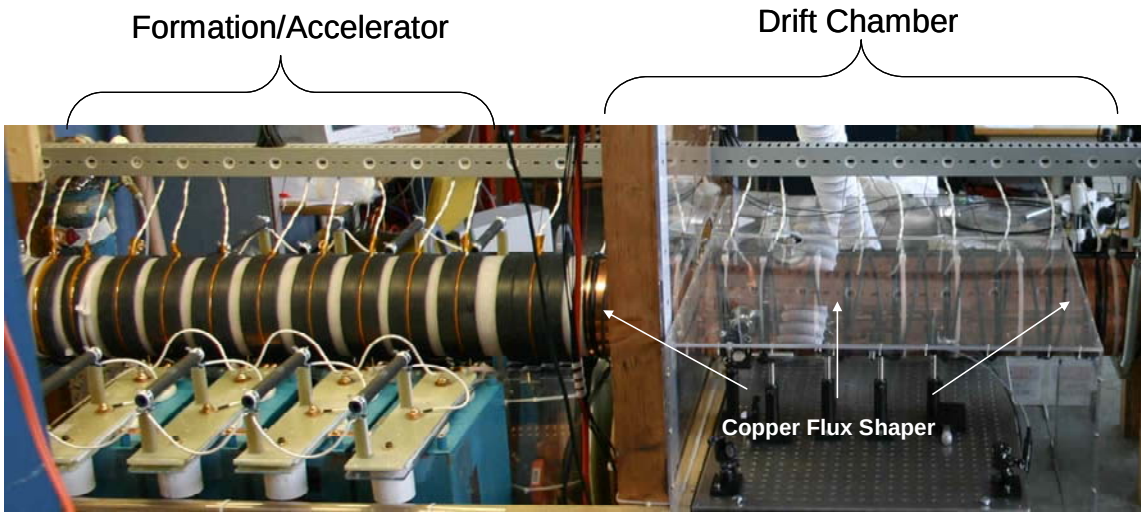

Figure 13. MAP accelerator magnetics. *Four of the 8 fast coil modules can be seen at left. The drift chamber magnetic field is produced by a single multi-turn winding running the length of the flux preserving (on the FRC transit timescale) single turn copper shell.*

B. Vacuum System

Given the size and complexity of the MAP prototype, it is fortunate that the vacuum need only extend to inside the coil boundaries. The vacuum wall is a cylinder of fused silica known as "Rotosil". Even though this type of fused silica is not transparent, it is structurally superior to clear quartz, and is not nearly as susceptible to shock stress. The tube was outfitted with large ISO flanges for connection to the main pumping/dump chamber on one end and the plasma gun start-up preionizer on the other. The entire system is maintained by a 1200 l/s turbo pump to a base pressure in the mid 10^{-8} Torr range, which is more than sufficient for the operation of the device without regard to background gasses. To obtain quality interferometric data, two 3 cm diameter holes were drilled into the side of the Rotosil tube in the drift section. Standard flanges were mounted over these holes to hold the window mounts for the cross tube interferometer. Two smaller holes were also made to allow for internal magnetic and other probes. A Langmuir triple probe and a B-dot probe will be employed to characterize the initial startup preionization. Given the high directed energy of the FRC, probing the internal structure of the passing supersonic FRC will follow only after initial operation and optimization studies have been completed.

C. Diagnostics

The most critical parameters for determining the FRC thrust is a determination of the FRC mass and velocity. Information about the FRC velocity can be obtained in a variety of ways. Essentially, every B loop will readily record the passage of the high β FRC. As was already mentioned, the FRC equilibrium size, shape, and velocity can be determined from a simple, passive, external array of magnetic loops. Fan arrays measuring plasma emission will be used to obtain the relative distribution of plasma density within the FRC through tomographic inversion. It is essential that these measurements be tied to an absolute measurement of density which will be provided by the optical interferometer. With this measurement, an accurate measure of the total FRC mass can be obtained as it passes. The equilibrium constraints (Eqs. (3) - (5)) allow for the determination of the FRC plasma temperature and internal energy as well. The FRC is unique in this way in that a very good knowledge of the key plasma parameters can be obtained from a few external measurements.

The Helium-Neon laser interferometer is in a Mach-Zender configuration. It is mounted on an optical table that straddles the tube providing beam stability. A Bragg cell is used to split the beam and for modulation, and no measurable fringe motion is observed on the time scale of the experiment. The scene beam is a double pass for improved sensitivity. It is believed that the system has a sensitivity sufficient for the line density to be accurately measured to a few percent. A 16 channel PMT-based Doppler spectrometer is available for measurement of T_i as well as FRC motion. It is capable of resolving the ion temperature to a few eV. This will be useful in determining the frozen flow conditions. The measurement can look across as well as down the axis of the accelerator.

IV. Conclusions and Future Work

With the completed assembly of the MAP thruster, the next step is clear. If the results are as expected, the MAP thruster prototype will produce an FRC with a directed energy of greater than 2 kJ per pulse at an Isp ~ 20,000 s. If the same rep rate were achieved with MAP as IMPAC (10 kHz), the jet power would be 2 kJ x 10^4/sec = 20 MW. With the formation, acceleration, and ejection of the FRC taking less than 10 μsec, this rep rate would still represent a duty cycle of no more than 10%. Before this result can be achieved there are clearly a few additional challenges to be met. There is the testing of the magnetic nozzle, and its effectiveness in reducing the frozen flow losses. A dielectric chamber of a sufficient size (0.8 m diameter, 2.7 m long) is available for this additional step for obtaining a higher thruster efficiency. The MAP prototype thruster has been designed to mate to this chamber. Various magnetic nozzle shapes and fields would be mounted inside this chamber at one end. The nozzle fields required are quite small. The maximum field at the throat of the nozzle employed in the numerical calculation shown in Fig. 6 was only 0.05 T (500 G). The large chamber can be operated with an axial magnetic guide field for evaluation of the thrust and Isp on the greatly expanded FRC in much the same way it will be done on the current device. There is also the task of operation with a true propagating wave electrical configuration in a repetitive mode. At first this would by necessity be limited to a series of a several pulses as it was on IMPAC, but the technology can be developed. Such a test would clearly demonstrate the feasibility of the high power MAP thruster.

Acknowledgments

This research is being supported by the United States Air Force Research Laboratory, Edwards Air Force Base.

References

[1]E.Y. Choueiri and J.K. Ziemer, "Quasi-Steady Magnetoplasmadynamic Thruster Database", *Journal of Propulsion and Power,* Vol. 17, No. 5, 2001, pp. 9673.

[2]C.L. Dailey and R.H. Lovberg, *The PIT MkV pulsed inductive thruster*, Technical Report NASA CR-191155, TRW Systems Group, July 1993.

[3]Maecker, H., "Plasma Jets in Arcs in a Process of Self-Induced Magnetic Compression," *Zeitschrift fur Physik*, Vol. 141, No. 1, 1955, pp. 198–216.

[4]Mikellides, P.G., "Modeling and Analysis of a Megawatt-Class Magnetoplasmadynamic Thruster", *Journal of Propulsion and Power,* Vol. 20, No. 2, 2004, pp. 204.

[5]J.T. Slough, et al., "Confinement and Stability in a Field-Reversed Configuration", *Phys. Rev. Lett*., Vol. 69, 1992, pp. 2212.

[6]M. Tuszewski, "Field Reversed Configurations", *Nuclear Fusion* Vol. 28**,** 1988 pp. 2033

[7]J.T. Slough, "Megawatt Plasma Thruster Based On An Inductive Plasma Accelerator (IMPAC)", Space Technology and Applications International Forum, Albuquerque, NM, January, 2000.

[8]S. Koelfgen, C. Hawk, R. Eskridge, M. Lee, A. Martin, and J. Smith, "A Plasmoid Thruster for Space Propulsion", AIAA-2003-4992, 39th AIAA/ASME/SAE/ASEE Joint Propulsion Conference and Exhibit, Huntsville, Alabama, July 20-23, 2003.

[9]D.J. Rej et al., "Experimental studies of field-reversed configuration translation",*Phys. Fluids,* Vol. 29, 1986, pp. 852

[10]R.D. Milroy and J.U. Brackbill, "Numerical studies of a field-reversed theta-pinch plasma", *Phys. Fluids,* Vol. 25, 1982, pp. 775

[11]J.T. Slough, "*Rapid Manned Mars Mission With a Propagating Magnetic Wave Plasma Accelerator",* NASA Institute for Advanced Concepts, Final Report (2000), www.niac.usra.edu.

[12]Hiroshi Gota, Kayoko Fujimoto, Yasunori Ohkuma, Tsutomu Takahashi, and Yasuyuki Nogi, "Separatrix shapes and internal structures of a field-reversed configuration plasma", *Physics of Plasmas*, Vol. 10, No. 12, 2003, pp. 4763.